Imaging of Tumor Angiogenesis Using ^{99m}Tc-Labeled Human Recombinant Anti-ED-B Fibronectin Antibody Fragments

Dietmar Berndorff[1], Sandra Borkowski[1], Dieter Moosmayer[1], Francesca Viti[2], Beate Müller-Tiemann[1], Stephanie Sieger[1], Matthias Friebe[1], Christoph S. Hilger[1], Luciano Zardi[3], Dario Neri[4], and Ludger M. Dinkelborg[1]

[1]Research Laboratories, Schering AG, Berlin, Germany; [2]Philogen S.p.A, Siena, Italy; [3]Department of Experimental and Clinical Immunology, Istituto Giannina Gaslini, Advanced Biotechnology Center, Genoa, Italy; and [4]Department of Chemistry and Applied Biosciences, Swiss Federal Institute of Technology, Zürich, Switzerland

The aim of this study was to target the angiogenesis-associated extracellular matrix protein ED-B fibronectin for molecular imaging of solid tumors. Recombinant and chemically modified derivatives of the single-chain antibody fragment (scFv) L19, capable of being labeled with ^{99m}Tc, were synthesized and radiolabeled. The resulting compounds ^{99m}Tc-AP39, ^{99m}Tc-L19-His, and ^{99m}Tc-L19-Hi20 were assessed for their imaging properties in vivo. **Methods:** L19 was genetically modified by inserting either the $(Gly)_3$-Cys-Ala (AP39) or a $(His)_6$ tag (L19-His) sequence at the C-terminal end. Chemical modifications were performed by conjugating the bifunctional chelator Hi20 (L19-Hi20) at ε-Lys-NH_2 residues of the molecule to allow for a direct chelator-based labeling with ^{99m}Tc. Tumor-targeting, pharmacokinetic, and scintigraphic imaging properties of the radiolabeled scFvs were evaluated in nude mice bearing murine F9 teratocarcinoma. **Results:** ^{99m}Tc labeling of the L19 derivatives yielded radiochemically pure proteins maintaining high immunoreactivity to ED-B fibronectin, as measured by affinity chromatography. Size-exclusion high-performance liquid chromatographic analysis of labeled L19 derivatives demonstrated either dimeric species (L19-His) or a mixture of predominantly associative dimeric and monomeric species (AP39, L19-Hi20). ^{99m}Tc-AP39 showed the most favorable biodistribution and imaging properties with high and fast tumor uptake (8.3 percentage injected dose per gram at 3 h after injection), rapid blood clearance and renal excretion, leading to high signal-to-noise ratios (tumor-to-blood ratio of 6.4 at 3 h after injection), and excellent planar scintigraphy in vivo. **Conclusion:** ED-B fibronectin can be efficiently targeted by ^{99m}Tc-AP39 and scintigraphically visualized in tumor-bearing mice, providing a potentially useful clinical tool for imaging of angiogenesis-associated ED-B fibronectin–expressing human tumors.

Key Words: molecular imaging; scintigraphy; ED-B fibronectin; angiogenesis; ^{99m}Tc labeling

J Nucl Med 2006; 47:1707–1716

Angiogenesis, characterized by the proliferation of new blood vessels from the preexisting vasculature, is a fundamental pathophysiologic feature of aggressive tumors and other relevant disorders (*1*). The recognition of the importance of angiogenesis to tumor growth and metastasis has led to enormous efforts in the pharmaceutical community to develop new drugs that are targeted to angiogenic vasculature. However, clinical development of antiangiogenic therapies has proven to be complex and challenging, making the requirement for imaging of surrogate biomarkers for early assessment of angiogenic inhibitors highly desirable (*2*). Functional characterization of the tumor neovasculature by molecular imaging would help to fulfill this need and, thereby, be an important clinical tool for therapy planning (patient stratification) and early therapy monitoring. Moreover, because of observed correlations between increased angiogenic activity and the likelihood of metastasis, progression of disease, or poorer prognosis, imaging of tumor angiogenesis even has the potential to serve as a prognostic parameter.

Fibronectin is a universal cell-adhesion molecule and represents the most widely distributed extracellular matrix protein. The splice variant ED-B fibronectin, containing the extra domain B, is an oncofetal antigen expressed at different levels in the stroma associated with the neovasculature of solid tumors and, thereby, known as a marker of angiogenesis (*3*). Its expression is restricted to angiogenic processes in embryonic development and tumorigenesis. In contrast, it is undetectable in most mature vessels and normal adult tissues, except for tissues undergoing physiologic remodeling, such as endometrium and ovaries (*4,5*). High levels of ED-B expression can be detected in primary tumors as well as metastatic lesions of almost all human solid cancer entities, including breast, colorectal, and non–small cell lung cancer (*6–8*). Therefore, targeting ED-B fibronectin for in vivo imaging purposes has the potential to serve not only as a general early tumor marker in tumorigenesis but also play a role as a surrogate parameter for

Received Apr. 7, 2006; revision accepted Jun. 28, 2006.
For correspondence or reprints contact: Dietmar Berndorff, PhD, Schering AG, Müllerstrasse 178, D-13342 Berlin, Germany.
E-mail: dietmar.berndorff@schering.de

monitoring and predicting the success of antiangiogenic cancer therapy.

L19 is a single-chain antibody fragment (scFv) that specifically targets the ED-B sequence of fibronectin and was first identified by Pini et al. (*9*). L19 was isolated from a phage display library of a synthetic human antibody repertoire binding to ED-B fibronectin with high affinity in the subnanomolar range (dissociation constant = 54 pmol/L). Specific accumulation of ^{125}I-L19 around tumor neovasculature and in tumor stroma correlated with ED-B fibronectin expression as subsequently demonstrated by microautoradiography analysis (*10*). ^{125}I-L19 showed specific tumor targeting combined with a fast blood clearance (*10,11*) in mice. Recently, ^{123}I-L19 was used for scintigraphic detection of ED-B fibronectin in cancer patients (*8*). In this study it was shown that ^{123}I-L19 selectively localized in tumor lesions of aggressive lung cancer as well as in liver metastases of colorectal cancer patients, directly correlating with the ED-B fibronectin expression. However, the use of radioactive iodine for in vivo imaging—except for thyroid imaging with iodide—is mainly hampered by the inconvenient labeling procedure (i.e., on-site preparation using kit chemistry is not feasible), the high costs, and the chemical instability due to dehalogenation. Therefore, we wished to introduce ^{99m}Tc as a more advantageous isotope for scintigraphic imaging into the protein. ^{99m}Tc is characterized by optimal physical properties, such as a half-life of 6 h, a nearly monoenergetic γ-emission of 140 keV, and its instant availability through a generator system.

Herein we describe the synthesis, ^{99m}Tc labeling, and in vivo characterization of the scFv L19 with altered labeling positions and radiometal chelating moieties. Because of the thiophilic nature of Tc(V), a free sulfhydryl group had to be introduced into the protein sequence for stable radiometal binding. Therefore, the amino acid sequence $(Gly)_3$-Cys-Ala was genetically inserted at the C terminus of L19, resulting in a recombinant protein named AP39, which is suitable for the direct labeling with ^{99m}Tc. In this molecule, technetium can form a Tc(V) oxo metal complex with, for example, 3 amide nitrogen atoms and 1 thiol sulfur atom in the Gly-Gly-Cys sequence (*12*) as 1 possible coordination mode. In a second approach, a $(His)_6$ tag was genetically introduced (L19-His) at the C terminus of the protein for direct ^{99m}Tc labeling with a Tc(I) carbonyl core (*13*). The Tc(V)O-core is also known to form stable complexes with mercaptoacetylglycine derivatives (MAG2 or MAG3), which can be conjugated efficiently to biomolecules (*14*). Hence, in a third approach, L19 was chemically modified by a bifunctional MAG2-type chelator (Fig. 1), conjugated to the ε-amino groups of Lys-residues of the scFv (L19-Hi20), and radiolabeled with ^{99m}Tc.

In vivo studies were performed with ^{99m}Tc-labeled AP39, L19-His, and L19-Hi20 in F9 tumor–bearing mice to investigate their ED-B fibronectin targeting potential and to compare their characteristics in biodistribution, pharmacokinetic, and imaging properties. The data clearly revealed the feasibility of targeting ED-B fibronectin for imaging tumors and the high potential of ^{99m}Tc-AP39 as the best-suited candidate for scintigraphy of angiogenesis-associated ED-B fibronectin in tumors.

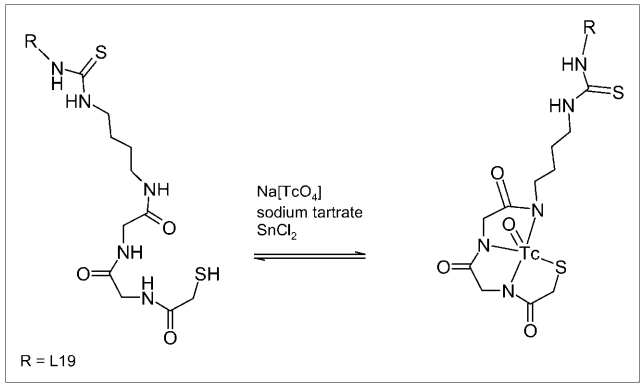

FIGURE 1. Synthesis scheme of ^{99m}Tc labeling of L19-Hi20.

MATERIALS AND METHODS

Protein Expression in *Escherichia coli*

For the production of L19 derivatives, the sequence of scFv L19 (*9*) was modified to encode either the ^{99m}Tc binding motif $(Gly)_3$-Cys-Ala (AP39) or the $(His)_6$ domain (L19-His) at the C-terminal end of the V_L chain. The DNA sequences encoding these L19 derivatives were cloned into the prokaryotic expression vector pDN5 (*9*) with isopropyl-1-thio-β-D-galactoside (IPTG)–inducible promoter and ampicillin resistance marker. All L19 derivatives used in this study are schematically shown in Figure 2. To allow secretion of the recombinant protein into the periplasm, the vector encoded an expression cassette in which the N terminus of scFv was fused to a Pel B signal sequence. This plasmid was transformed into *E. coli* TG1 for generation of a producer strain. The *E. coli* preculture was incubated at 37°C in 2× YT medium containing 100 μg/mL ampicillin and 1% glucose for 16 h. For production, a shaker flask with medium (2× YT medium, 0.1% glucose, 100 μg/mL ampicillin) was inoculated with 1/100 volume preculture and incubated at 30°C. The culture was induced with 1.5 mmol/L IPTG after reaching an optical density (OD_{550}) of 0.8–1.0 and was further incubated for 16 h. Soluble and binding active scFv protein could be isolated from the soluble fraction of the French press lysate of the *E. coli* culture, from the periplasmic fraction, or from the culture supernatant—which proved to be particularly efficient in relation to purification and yield. Production took place in shaker flasks and in fermenters with a culture volume of up to 10 L.

The culture supernatant was decanted and the L19 derivatives were purified by affinity chromatography (protein A, immobilized metal, or ED-B antigen column). The scFv L19 was purified by ED-B affinity chromatography according to Pini et al. (*9*). AP39 was eluted from the protein A column using a buffer consisting of 100 mmol/L Na_2PO_4, 300 mmol/L NaCl, and 10% glycerol (adjusted to pH 3.5 with citric acid). L19-His bound to the immobilized metal column was eluted with triethylamine (pH 11). The eluted samples were adjusted to pH 8 using Tris base. The fractions containing the scFvs were further concentrated and purified by size-exclusion (SE) chromatography (Superdex 75; Amersham Biosciences). The protein concentration was determined by

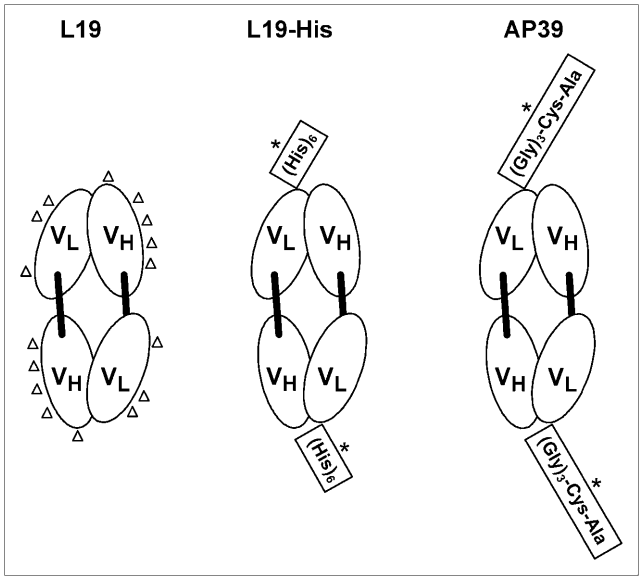

FIGURE 2. Schematic drawings show domain structure and potential ^{99m}Tc acceptor sites of antibody derivatives that were investigated in this study. Derivatives consist of V_L and V_H domains of L19 scFv. Using a bifunctional chelator, L19 can be labeled indirectly with ^{99m}Tc (potential ^{99m}Tc acceptor sites suitable for indirect labeling are indicated by triangles). By insertion of the peptide sequence $(His)_6$ and $(Gly)_3$-Cys-Ala in L19-His and AP39, respectively, these molecules can be labeled directly with ^{99m}Tc (potential ^{99m}Tc acceptor sites suitable for direct labeling are indicated by asterisks).

measurement of the optical density and the protein was stored at 4°C until radiolabeling was performed.

Radiolabeling with ^{99m}Tc

General Procedures. All chemicals were purchased from Fluka, Aldrich, or Merck and were used without further purification. Sodium pertechnetate ^{99m}Tc was obtained on the day of use from an ElumaticIII-8 ^{99}Mo/^{99m}Tc-generator (CIS-Bio-International). High-performance liquid chromatographic (HPLC) analysis of radiolabeled L19 derivatives was performed on a Biotek system (BioTek Instruments), equipped with a radioflow HPLC detector (EG & G Bertold). Samples were injected onto TSK-Gel size-exclusion columns (Tosoh Haas) and eluted with buffer (0.1 mol/L Na_2HPO_4, 0.1 mol/L Na_2SO_4, 0.05% NaN_3, pH 6.7) at a flow rate of 0.4 mL/min. Elution was monitored by ultraviolet detection at 275 nm (100 μL) and γ-detection (10 μL). A radioisotope dose calibrator (PTW-Dr. Pychlau GmbH) was used to determine the radioactive content of the labeling solutions. Small radioactive samples were counted on a γ-counter (Compugamma; LKB Wallac).

^{99m}Tc Radiolabeling of AP39. Before radiolabeling, AP39 had to be reduced by adding 83.3 μL Tris-(2-carboxyethyl)phosphine-hydrochloride (TCEP) solution (14.34 mg TCEP·HCl in 5 mL of 0.1 mol/L Na_2HPO_4 buffer, pH 7.4) to a solution of 400 μg purified AP39 in 140 μL phosphate-buffered saline (PBS)/10% glycerol (pH 7.4). The reaction mixture was gently shaken for 1 h at room temperature. TCEP was removed from the AP39 preparation by chromatography using a NAP-5 column (Sephadex G-25 DNA grade, eluent: PBS; Amersham Biosciences). Sodium dodecyl sulfate/polyacrylamide gel electrophoresis of the isolated product confirmed the quantitative transformation of S–S-dimeric AP39 to AP39 in the SH-monomer and associative dimer form. Protein yields of 136 μg/180 μL PBS could be achieved. For radiolabeling, 4.2 mg disodium-L-tartrate were placed in a 2-mL glass-vial followed by addition of 136 μg reduced AP39 in 180 μL PBS. The solution was diluted with 100 μL aqueous Na_2HPO_4 buffer (1 mol/L, pH 10.5) and 100 μL ^{99m}Tc generator eluate plus 10 μL tin-II chloride solution (5 mg $SnCl_2$, 1 mL of 0.1 mol/L HCl) were added. The reaction mixture was shaken for 30 min at 37°C. ^{99m}Tc-AP39 was purified by gel chromatography using a NAP-5 column (Sephadex G-25 DNA grade, eluent: PBS). The ^{99m}Tc-compound was protected against air oxidation by adding 2 μL tin-II chloride solution (5 mg $SnCl_2$, 1 mL of 0.1 mol/L HCl). The radiochemical yield and purity were determined by SE-HPLC. Therefore, a Tosoh Haas, TSK-Gel SWxL2000 SE column (300 × 7.8 mm) was eluted with an isocratic flow (0.5 mL/min) of aqueous Na_2HPO_4/Na_2SO_4 (0.1 mol/L) buffer solution (1:1, v/v), completed with 0.05% NaN_3 (pH 6.7).

^{99m}Tc Radiolabeling of L19-His. Radiolabeling of L19-His was performed by applying the tricarbonyl method as described earlier (*14*) using $[^{99m}Tc(OH_2)_3(CO)_3]^+$. Quality control of the synthesized $[^{99m}Tc(OH_2)_3(CO)_3]^+$ was performed by gradient HPLC, injecting 20 μL (2 MBq/mL) on a Eurospher 100-C18 column (250 × 4 mm; Knauer GmbH) and eluting with a gradient of 0.05 mol/L triethylammoniumphosphate (pH 2.25) (A) and MeOH (B) (0% B to 100% B within 20 min). To radiolabel L19-His with $[^{99m}Tc(OH_2)_3(CO)_3]^+$, 100 μg of the protein (1.0 mg/mL scFv L19-His in 10 mmol/L *N*-(2-hydroxyethyl)piperazine-*N*′-(2-ethanesulfonic acid) buffer, pH 7.5, 150 mmol/L NaCl) were added to 200 μL PBS and 37 MBq $[^{99m}Tc(OH_2)_3(CO)_3]^+$ solution (31 μL). The mixture was incubated for 1 h at 37°C and the ^{99m}Tc-L19-His product was purified by affinity chromatography using a NAP-5 column (eluent: PBS). The radiolabeled compound was analyzed by SE-HPLC as described.

^{99m}Tc Radiolabeling of L19-Hi20. The chelator Hi20 (2-tert-butyldisulfanyl-*N*-({[(4-isothiocyanatobutylcarbamoyl)methyl] carbamoyl}-methyl)acetamide) was conjugated to ε-NH_2 groups of L19 by dissolving 2 mg of L19 in 1.3 mL PBS and dialyzing twice with sodium borate buffer (200 mL, 0.1 mol/L, pH 8.5) in a Slide-A-Lyzer (equipped with a 10-kDa molecular weight cutoff membrane; Pierce Chemicals). Hi20 (1.5 mg) was dissolved in *N*,*N*-dimethylformamide (150 μL) and added to the protein solution. The mixture was incubated for 3 h at 37°C. The solution was allowed to cool to room temperature for 10 min and was then dialyzed with PBS (400 mL, 0.1 mol/L, pH 7.4) 3 times for 1 h and once overnight. Before radiolabeling, the protein–chelator conjugate was reduced by the addition of TCEP (150 μL, 0.1 mol/L, pH 7.4) and incubation at 37°C for 1 h The sample was purified on a NAP-5 column, preeluted with PBS/0.5% bovine serum albumin (BSA), and, finally, eluted with PBS (3 × 3 mL). For radiolabeling, 110 μg L19-Hi20 (in 310 μL PBS) were supplemented with 3.3 mg sodium tartrate dihydrate, phosphate buffer (100 μL, 1.0 mol/L, pH 10.5), ^{99m}Tc generator eluate (70 MBq, 50 μL, sodium pertechnetate (VII)), and stannous (II) chloride (10 μL, stock solution: 5 mg $SnCl_2$ in 1 mL of 0.1 mol/L HCl). The mixture was incubated at 37°C for 30 min and purified on a NAP-5 column that was preeluted with PBS/0.5% BSA. The product was finally eluted with PBS (3 × 3 mL). An addition of 5 μL of stannous (II) chloride solution completed the procedure to stabilize the product. Analysis followed by SE-HPLC.

Immunoreactivity

Assessment of immunoreactivity of ^{99m}Tc-L19 derivatives was performed by affinity chromatography according to Tarli et al. (*10*) using a column containing ED-B fibronectin–conjugated Sepharose.

Cell Lines and Animals

Mouse embryonal teratocarcinoma cells (F9) were purchased from the American Tissue Culture Collection. The tumor cells were cultivated in Dulbecco's modified Eagle medium with Glutamax (Invitrogen), supplemented with 10% fetal calf serum (Invitrogen) and maintained at 37°C in 5% CO_2 in air. To induce tumors, female nude mice (NMRI *nu/nu*; Taconic), weighing 20−25 g, were injected subcutaneously with 1×10^6 F9 cells in a volume of 100 μL PBS with Ca^{2+}/Mg^{2+} (Invitrogen) into the right hind limb. After 11 d, tumors reached a size of approximately 0.8 cm in diameter and the animals were used for biodistribution and imaging experiments. All animal experiments were performed in compliance with the current version of the German law on the Protection of Animals.

Biodistribution Studies

Tumor-bearing mice were injected intravenously in the tail vein with approximately 74 kBq of ^{99m}Tc-L19 derivatives. Three mice per time point were sacrificed at 15 min and at 1, 3, 5, and 24 h after injection for organ excision. In addition, urine and feces were collected over time. The dissected organs and collected excretions were counted for radioactivity in a γ-counter (Compugamma; LKB Wallac), and values of the percentage injected dose per gram (%ID/g) and the percentage injected dose (%ID) were calculated.

Imaging

Tumors were imaged when they reached an area of 80−100 mm^2. For imaging, conscious mice were injected intravenously in the tail vein with 4−7 MBq of ^{99m}Tc-L19 derivatives. The mice were anesthesized using subcutaneously injected rompun/ketamin (2:1 mL/kg) and images of each animal were taken at 5 and 24 h after injection. Imaging was performed using an SP-4 HR γ-camera (Elscint) with the following imaging parameters: energy, 140 keV; rate mode, normal; collimator, 4; static; frame size, 256; zoom, 2; rotation, 180°; view, posterior.

RESULTS

Production of ED-B–Specific Recombinant ScFv Antibody Molecules

In addition to the anti–ED-B fibronectin scFv L19, we generated two recombinant L19 derivatives comprising different C-terminal tags for site-specific radiolabeling: AP39, which encodes a tag with the sequence $(Gly)_3$-Cys-Ala, and L19-His, which contains a $(His)_6$ tag. The scFvs AP39 and L19-His were expressed in *E. coli* as soluble proteins that accumulated in the culture supernatant. Approximately 5 mg of L19-His and 0.5 mg of AP39 were excreted per liter of culture supernatant.

^{99m}Tc Labeling of L19 Derivatives

^{99m}Tc Labeling of AP39. Immediately before radiolabeling, the purified AP39 was reduced with TCEP. The radiolabeling procedure, using the purified and TCEP-reduced AP39, with ^{99m}Tc gave radiochemical yields of >50% (NAP-5 column purified). A radiochemical purity of >95% was observed, as determined by SE-HPLC analysis. The product is present as a mixture of predominantly dimeric (~81%) and monomeric (~16%) ^{99m}Tc-AP39, as determined by SE-HPLC (Fig. 3). ED-B affinity chromatography revealed an immunoreactivity of 96%. The specific activity of ^{99m}Tc-AP39 was 35 MBq/nmol (dimer).

^{99m}Tc Labeling of L19-His. Radiolabeling of L19-His with the $[^{99m}Tc(OH_2)_3(CO)_3]^+$ labeling precursor led to the

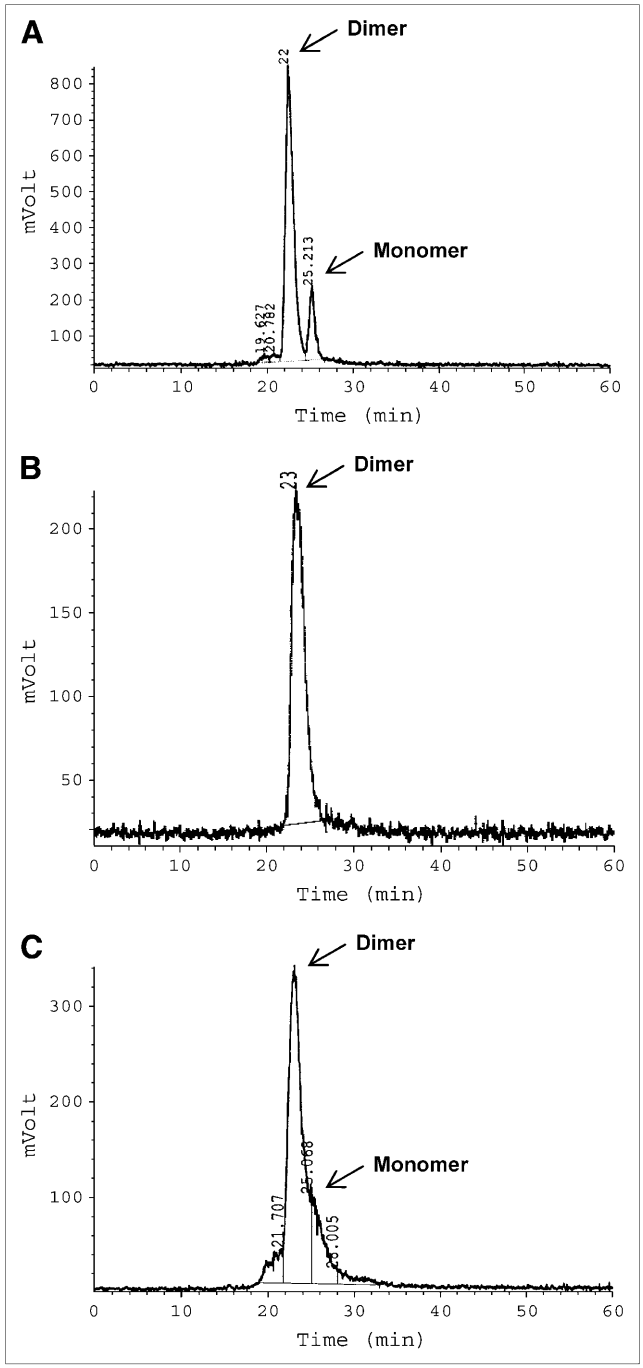

FIGURE 3. Representative SE-HPLC chromatograms (radiation detection) of ^{99m}Tc-AP39 (A), ^{99m}Tc-L19-His (B), and ^{99m}Tc-L19-Hi20 (C).

formation of ^{99m}Tc-L19-His conjugates with a radiochemical yield of 47% and a purity of >93%, as determined by SE-HPLC analysis. The specific activity of ^{99m}Tc-L19-His was 9 MBq/nmol (dimer). ^{99m}Tc-L19-His was detected as a dimer by SE-HPLC analysis (Fig. 3). The immunoreactivity of ^{99m}Tc-L19-His was 89%, as measured by ED-B affinity chromatography.

^{99m}Tc Labeling of L19-Hi20. ^{99m}Tc labeling of L19 via the bifunctional chelator Hi20 resulted in a radiochemical yield of 54% and a radiochemical purity of >91%. The specific activity was 21 MBq/ nmol (dimer). NAP-5 purification yielded ^{99m}Tc-19-Hi20 as a monomer/dimer mixture, as monitored by SE-HPLC (Fig. 3). However, a complete separation of the dimeric and monomeric format could not be achieved by this HPLC method. The immunoreactivity was 82%, as measured by ED-B affinity chromatography.

Biodistribution Data

Biodistribution experiments with the ^{99m}Tc-L19 derivatives AP39, L19-His, and L19-Hi20 were performed over 24 h in nude mice bearing the murine teratocarcinoma F9 (Tables 1–3).

All three radioimmunoconjugates investigated in this study showed selective ED-B targeting in F9 tumors but also accumulated in the ED-B fibronectin–expressing reproductive organs, ovaries and uterus. For ^{99m}Tc-AP39, a rapid tumor uptake was observed with a maximum of 8.7 %ID/g after 5 h, decreasing to 2.8 %ID/g at 24 h after injection (Fig. 4A). The rapid tumor localization of ^{99m}Tc-AP39, combined with its fast blood clearance (Fig. 4B), led to a tumor-to-blood ratio (T/B ratio) of 6.4 after 3 h following injection, increasing to 17.2 after 24 h (Table 1). With the exception of the kidneys, there was no nonspecific accumulation of radioactivity in nontarget organs. Kidney uptake, which is attributed to the renal elimination of the compound (64.5 %ID of ^{99m}Tc-AP39 is excreted via the urine after 24 h), was highest at 48.2 %ID/g after 0.25 h following injection and decreased to 2.6 %ID/g after 24 h. The absence of radioactivity in the thyroid and bone indicated no significant release of ^{99m}Tc-pertechnetate from the

TABLE 1
Biodistribution of ^{99m}Tc-AP39 in F9 Tumor–Bearing Mice

Tissue	Biodistribution time (h)				
	0.25	1	3	5	24
Uptake (%ID/g)					
Spleen	5.1 ± 0.7	2.0 ± 0.3	0.7 ± 0.2	0.6 ± 0.1	0.2 ± 0.0
Liver	5.1 ± 0.2	2.5 ± 0.3	1.1 ± 0.2	1.1 ± 0.2	0.3 ± 0.0
Kidneys	48.2 ± 4.2	21.8 ± 2.5	8.6 ± 0.6	7.9 ± 0.4	2.6 ± 0.4
Lung	6.9 ± 1.7	3.1 ± 0.2	1.2 ± 0.0	1.1 ± 0.2	0.8 ± 1.0
Bone*	2.8 ± 0.9	2.3 ± 0.3	1.6 ± 0.2	1.7 ± 0.1	0.8 ± 0.2
Heart	4.1 ± 1.3	1.8 ± 0.2	0.7 ± 0.2	0.4 ± 0.0	0.2 ± 0.0
Brain	0.4 ± 0.0	0.1 ± 0.0	0.1 ± 0.0	ND	ND
Thyroid	3.4 ± 0.6	2.0 ± 0.2	1.3 ± 0.1	1.3 ± 0.7	0.8 ± 0.4
Muscle*	0.8 ± 0.1	0.6 ± 0.0	0.6 ± 0.2	0.2 ± 0.0	0.1 ± 0.0
Stomach†	1.7 ± 0.1	1.4 ± 0.0	1.1 ± 0.1	1.0 ± 0.0	0.4 ± 0.1
Intestine‡	1.6 ± 0.1	1.4 ± 0.0	1.3 ± 0.2	1.6 ± 0.5	0.3 ± 0.0
Uterus	2.5 ± 0.8	2.0 ± 0.5	1.4 ± 0.7	2.8 ± 1.2	1.3 ± 0.7
Ovaries	13.0 ± 1.8	7.6 ± 2.2	4.3 ± 1.4	2.7 ± 0.9	0.9 ± 0.1
Tumor	5.2 ± 2.5	6.1 ± 2.0	8.3 ± 3.2	8.7 ± 5.5	2.8 ± 1.4
Blood	14.4 ± 0.9	3.9 ± 0.8	1.3 ± 0.1	1.0 ± 0.1	0.2 ± 0.0
Excretion (%ID)					
Urine	22.7 ± 3.9	46.7 ± 4.4	48.8 ± 6.7	52.5 ± 2.0	64.5 ± 6.5
Feces	ND	ND	0.4 ± 0.1	0.6 ± 0.5	4.8 ± 1.0
Tumor/tissue ratio					
T/spleen	1.0 ± 0.3	3.1 ± 0.6	12.4 ± 7.3	14.8 ± 11.4	11.5 ± 4.5
T/liver	1.0 ± 0.4	2.4 ± 0.5	7.8 ± 4.0	8.3 ± 6.2	8.1 ± 3.6
T/kidneys	0.1 ± 0.0	0.3 ± 0.1	1.0 ± 0.4	1.1 ± 0.8	1.0 ± 0.4
T/lung	0.8 ± 0.5	2.0 ± 0.7	6.8 ± 2.6	8.3 ± 6.5	7.5 ± 5.9
T/muscle	6.8 ± 3.4	10.5 ± 3.2	13.6 ± 2.6	38.5 ± 28.9	25.3 ± 11.2
T/blood	0.4 ± 0.2	1.6 ± 0.2	6.4 ± 2.9	9.0 ± 6.5	17.2 ± 6.8
T/intestine	3.3 ± 1.3	4.3 ± 1.3	6.9 ± 3.6	6.9 ± 6.9	8.9 ± 3.7

*Tissue aliquot only.
†Without content.
‡With content.
ND = not detectable; T = tumor.
All data are presented as mean ± SD (n = 3).

TABLE 2
Biodistribution of ^{99m}Tc-L19-His in F9 Tumor–Bearing Mice

Tissue	Biodistribution time (h)				
	0.25	1	3	5	24
Uptake (%ID/g)					
Spleen	5.5 ± 0.6	2.7 ± 0.7	1.8 ± 0.2	1.2 ± 0.2	0.8 ± 0.2
Liver	6.1 ± 0.7	3.4 ± 0.4	4.3 ± 0.3	3.4 ± 0.7	2.5 ± 0.7
Kidneys	87.5 ± 5.2	124.7 ± 6.3	145.1 ± 22.3	117.0 ± 12.9	72.4 ± 11.3
Lung	10.4 ± 1.8	5.2 ± 1.0	4.0 ± 1.2	4.1 ± 2.9	2.0 ± 0.6
Bone*	4.6 ± 0.9	5.4 ± 1.0	2.9 ± 1.5	3.4 ± 0.7	3.1 ± 0.9
Heart	5.2 ± 0.2	2.3 ± 0.2	1.1 ± 0.1	0.7 ± 0.1	0.4 ± 0.1
Brain	0.4 ± 0.1	0.2 ± 0.0	0.1 ± 0.0	0.1 ± 0.0	0.1 ± 0.0
Thyroid	4.9 ± 1.5	2.9 ± 0.1	2.7 ± 1.3	2.7 ± 1.1	1.1 ± 0.0
Muscle*	0.5 ± 0.2	0.6 ± 0.1	0.6 ± 0.1	0.4 ± 0.1	0.3 ± 0.1
Stomach†	2.0 ± 0.2	1.7 ± 0.1	2.1 ± 0.2	1.7 ± 0.3	1.1 ± 0.2
Intestine‡	1.4 ± 0.1	1.8 ± 0.2	2.4 ± 0.5	1.9 ± 0.8	1.2 ± 0.7
Uterus	3.2 ± 1.7	4.7 ± 1.3	4.9 ± 1.2	2.7 ± 0.8	4.4 ± 2.4
Ovaries	27.2 ± 18.8	10.2 ± 2.1	6.0 ± 1.0	6.9 ± 1.0	2.8 ± 0.5
Tumor	6.3 ± 2.0	8.4 ± 0.8	9.4 ± 1.4	8.1 ± 2.0	5.7 ± 2.0
Blood	18.7 ± 2.0	4.3 ± 0.1	1.7 ± 0.3	0.9 ± 0.1	0.2 ± 0.1
Excretion (%ID)					
Urine	10.8 ± 3.3	14.8 ± 5.4	20.9 ± 5.5	21.3 ± 4.9	64.5 ± 6.5
Feces	ND	ND	0.2 ± 0.3	0.6 ± 0.3	4.8 ± 1.0
Tumor/tissue ratio					
T/spleen	1.2 ± 0.4	3.3 ± 1.1	5.3 ± 0.7	7.0 ± 2.3	6.6 ± 1.0
T/liver	1.1 ± 0.4	2.5 ± 0.5	2.2 ± 0.5	2.4 ± 0.6	2.3 ± 0.2
T/kidneys	0.1 ± 0.0	0.1 ± 0.0	0.1 ± 0.0	0.1 ± 0.0	0.1 ± 0.0
T/lung	0.6 ± 0.1	1.7 ± 0.4	2.5 ± 0.8	2.5 ± 1.2	2.9 ± 0.9
T/muscle	12.4 ± 1.4	15.5 ± 45	16.4 ± 4.2	23.0 ± 9.5	22.9 ± 6.6
T/blood	0.4 ± 0.1	2.0 ± 0.2	5.7 ± 0.5	9.5 ± 2.6	23.6 ± 8.3
T/intestine	4.5 ± 1.7	4.8 ± 0.9	4.0 ± 0.7	4.9 ± 2.2	4.9 ± 1.4

*Tissue aliquot only.
†Without content.
‡With content.
ND = not detectable; T = tumor.
All data are presented as mean ± SD (n = 3).

chelator, attesting to the radiochemical stability of the peptidergic ^{99m}Tc chelator. ^{99m}Tc-L19-His showed a slightly higher tumor uptake than AP39, with a maximum of 9.4 %ID/g already achieved at 3 h after injection (Fig. 4A). The fast blood clearance was similar to that of AP39 (Fig. 4B) and resulted in a high T/B ratio of 6.4 at 3 h after injection, which increased to 23.6 after 24 h. However, ^{99m}Tc-L19-His strongly accumulated in the kidneys with a maximum uptake of 145.1 %ID/g at 3 h after injection, decreasing to 72.4 %ID/g at 24 h (Table 2). Urinary excretion of ^{99m}Tc-L19-His (32.4 %ID after 24 h) was lower than that of AP39. Slightly increased levels of ^{99m}Tc-L19-His were measured in spleen, liver, lung, and bone compared with AP39 (Fig. 4C). Labeling of L19 with ^{99m}Tc via the bifunctional chelator Hi20 resulted in a marginally lower tumor accumulation (maximum, 7.7 %ID/g at 3 h) and a slower blood clearance of the compound compared with ^{99m}Tc-AP39 and ^{99m}Tc-L19-His (Figs. 4A and 4B). T/B ratios were 2.7 at 5 h after injection and 9.3 after 24 h. Compared with ^{99m}Tc-AP39, the kidney uptake of ^{99m}Tc-L19-Hi20 was initially lower but cleared more slowly over time (Table 3). Similar to L19-His, slightly elevated organ uptake was observed for L19-Hi20 in spleen, liver, lung, and bone (Fig. 4C).

Scintigraphy

Imaging studies in mice were performed at 5 and 24 h after injection of ^{99m}Tc-L19 derivatives. ^{99m}Tc-AP39 was additionally imaged at 3 h after injection. A specific accumulation of radioactivity in the tumor expressing the ED-B fibronectin target could be demonstrated by scintigraphic imaging of all three ^{99m}Tc-L19 derivatives (Figs. 5–7).

Scintigraphy with ^{99m}Tc-AP39 gave clear tumor images until 24 h after injection with low background activities (Fig. 5). As predicted from the biodistribution studies, the renal elimination of AP39 led to visualization of the kidneys at 3 and 5 h, which decreased after 24 h, whereas the tumor remained clearly visible. Liver and bladder were also weakly detected at early time points. Similar to AP39, tumors could be clearly depicted by ^{99m}Tc-L19-His–based imaging at 5 and 24 h after injection (Fig. 6). The background was low except for strong accumulation of

TABLE 3
Biodistribution of ^{99m}Tc-L19-Hi20 in F9 Tumor–Bearing Mice

Tissue	Biodistribution time (h)				
	0.25	1	3	5	24
Uptake (%ID/g)					
Spleen	4.9 ± 0.5	4.1 ± 0.7	2.8 ± 1.0	1.4 ± 0.2	0.5 ± 0.1
Liver	10.5 ± 2.1	7.1 ± 0.1	4.7 ± 0.6	3.4 ± 0.5	1.7 ± 0.2
Kidneys	33.5 ± 2.4	26.6 ± 0.7	15.2 ± 1.3	10.9 ± 0.4	3.0 ± 0.6
Lung	9.4 ± 1.4	6.2 ± 0.6	5.0 ± 1.8	2.6 ± 0.8	1.3 ± 0.5
Bone*	4.0 ± 0.4	4.2 ± 0.6	3.6 ± 0.5	2.9 ± 0.5	1.0 ± 0.1
Heart	4.7 ± 1.5	3.3 ± 0.4	1.6 ± 0.3	1.1 ± 0.1	0.2 ± 0.0
Brain	0.4 ± 0.1	0.3 ± 0.0	0.1 ± 0.0	0.1 ± 0.0	ND
Thyroid	3.5 ± 1.4	4.3 ± 1.2	1.9 ± 0.8	3.2 ± 1.1	0.7 ± 0.1
Muscle*	0.8 ± 0.2	0.7 ± 0.0	0.5 ± 0.1	0.5 ± 0.1	0.2 ± 0.0
Stomach†	1.9 ± 0.1	2.5 ± 0.2	1.6 ± 0.1	1.5 ± 0.1	0.6 ± 0.1
Intestine‡	1.6 ± 0.2	3.3 ± 0.2	4.4 ± 1.1	4.2 ± 1.8	0.9 ± 0.4
Uterus	2.1 ± 0.8	4.9 ± 1.5	3.8 ± 2.4	3.1 ± 0.9	1.6 ± 0.7
Ovaries	7.6 ± 4.1	8.4 ± 0.4	4.4 ± 0.8	3.6 ± 0.9	1.0 ± 0.2
Tumor	3.5 ± 0.6	6.8 ± 1.9	7.7 ± 2.1	7.6 ± 0.6	4.0 ± 2.6
Blood	16.1 ± 1.7	9.5 ± 0.2	4.3 ± 0.6	2.8 ± 0.3	0.4 ± 0.0
Excretion (%ID)					
Urine	19.1 ± 2.4	27.1 ± 6.0	38.8 ± 4.4	41.8 ± 4.0	57.8 ± 3.0
Feces	ND	ND	2.6 ± 1.3	7.3 ± 6.1	18.6 ± 4.0
Tumor/tissue ratio					
T/spleen	0.7 ± 0.1	1.7 ± 0.4	3.1 ± 1.4	5.4 ± 1.2	7.7 ± 5.7
T/liver	0.4 ± 0.1	1.0 ± 0.3	1.6 ± 0.4	2.2 ± 0.3	2.4 ± 1.9
T/kidneys	0.1 ± 0.0	0.3 ± 0.1	0.5 ± 0.2	0.7 ± 0.1	1.4 ± 1.0
T/lung	0.4 ± 0.0	1.1 ± 0.2	1.6 ± 0.5	3.1 ± 0.7	4.5 ± 4.9
T/muscle	4.8 ± 1.8	9.7 ± 3.1	17.5 ± 8.5	15.5 ± 2.1	25.7 ± 13.5
T/blood	0.2 ± 0.1	0.7 ± 0.2	1.8 ± 0.5	2.7 ± 0.4	9.4 ± 6.4
T/intestine	2.2 ± 0.4	2.1 ± 0.5	1.9 ± 0.8	2.0 ± 0.8	8.4 ± 2.8

*Tissue aliquot only.
†Without content.
‡With content.
ND = not detectable; T = tumor.
All data are presented as mean ± SD (n = 3).

^{99m}Tc-L19-His in the kidneys, which remained substantially visible until 24 h. Additionally, the liver was slightly detectable after 5 h. Scintigraphic images of ^{99m}Tc-L19-Hi20 (Fig. 7) showed accumulation of radioactivity in the tumor comparable with that of the 2 other L19 derivatives. The 5 h image displayed high background activities for ^{99m}Tc-L19-Hi20 in kidney and liver, which cleared after 24 h following injection, resulting in low background activity and a visible tumor.

DISCUSSION

The realization that angiogenesis is an essential step for tumor growth and for the initiation of metastases has led to substantial interest in the discovery of angiogenic factors and the development of new drugs that are targeted to the tumor angiogenic vasculature. However, clinical trials with these agents are challenging, because reproducible and reliable angiogenic markers for patient stratification are still missing and because of the long time it currently takes to determine whether such drugs have a clinical effect. Therefore, there is a need for rapid and effective biomarkers to help delineate prognosis and stratification for adjuvant treatments (both cytotoxic and antiangiogenic/targeted cytostatic) and to monitor specific clinical response early after the onset of therapy. ED-B fibronectin as a splice variant of fibronectin is typically expressed at sites of tissue remodeling. High levels of ED-B expression can be observed in primary tumor lesions as well as in metastatic sites of almost all human solid cancer entities but not in inflammatory tissue (*15*). Therefore, ED-B fibronectin–targeted imaging might serve as a biomarker for differential diagnosis, prognosis, and stratification in a variety of solid tumor patients.

Since the introduction of the anti-ED-B fibronectin scFv L19, several therapeutically active L19 conjugates have been investigated. For example, the fusion protein L19-TNF-α (TNF-α is tumor necrosis factor α) showed substantial inhibition of tumor growth in mice (*16*), and the cytokines interleukin 12 and TNF-α fused to the L19 protein demonstrated in combination the complete cure of tumor-bearing mice with only minor side effects (*17*). The

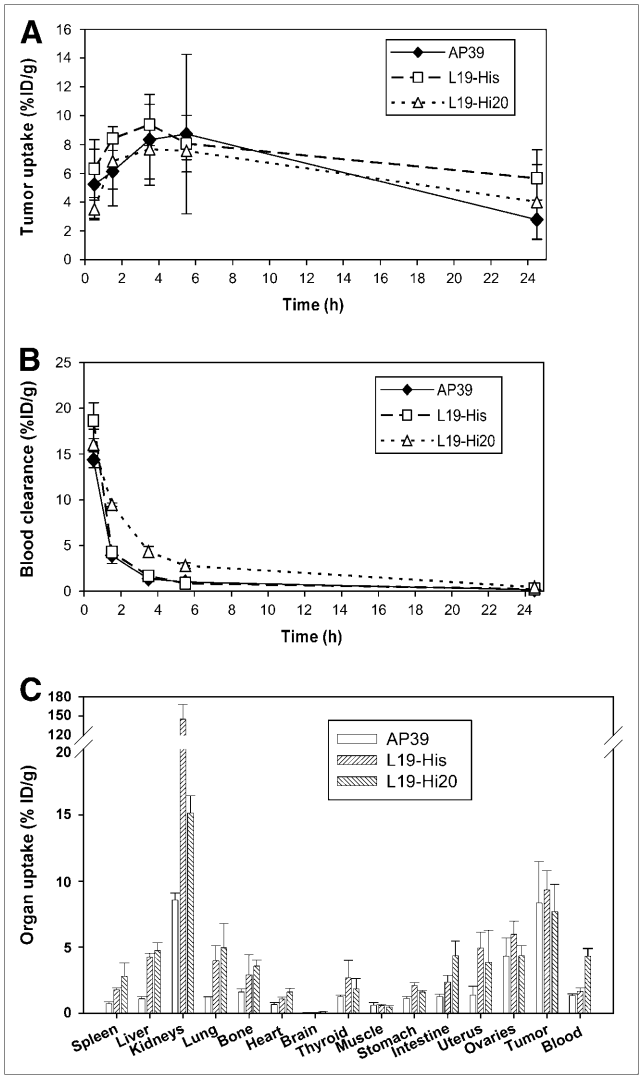

FIGURE 4. Comparison of ^{99m}Tc-L19 derivatives in F9 tumor–bearing nude mice with regard to tumor uptake up to 24 h after injection (A), blood clearance up to 24 h after injection (B), and organ uptake at 3 h after injection (C). All data are presented as mean ± SD (n = 3).

potential therapeutic use of L19 derivatives may trigger a clinical need of a diagnostic counterpart for imaging.

The targeting of ED-B fibronectin for imaging has already been investigated in a preliminary clinical study using ^{123}I-L19. Recurrent glioblastoma, small cell lung cancer, and a large liver metastasis of a colon carcinoma could be detected using the iodinated scFv (*8*). However, for clinical use, ^{99m}Tc is the preferred isotope compared with ^{123}I because of its shorter half-life (6 h), the convenient labeling procedure, and the optimal γ-energy. Being generator produced, ^{99m}Tc is inexpensive and readily available. If considering L19 as a targeting molecule, ^{99m}Tc offers the additional advantage that its physical half-life matches ideally the biologic half-life of the scFv. The creation of a ^{99m}Tc binding site by the conjugation of a chelator to the targeting molecule can be associated with instability of the labeled proteins (*18*), whereas attempts to genetically engineer cysteine groups into proteins may lead to problems with protein expression, folding, or stability (*19*). We have evaluated the direct and indirect ^{99m}Tc labeling approaches of L19, followed by in vivo investigations of tumor-targeting potential and pharmacokinetic behavior. Direct radiolabeling of L19 with technetium has been performed after creation of an intramolecular ^{99m}Tc binding site via genetically inserting the amino acid sequence $(Gly)_3$-Cys-Ala (AP39) or the $(His)_6$ domain (L19-His). Both derivatives could be expressed in *E. coli* in amounts that were sufficient for the studies described herein (i.e., 0.5 mg/L for AP39 and 5 mg/L for L19-His). For both AP39 and L19-His recombinant scFvs, the site-directed binding of ^{99m}Tc did not lead to a loss in immunoreactivity (>89%). As an alternative to the intramolecular direct labeling with ^{99m}Tc (AP39, L19-His), we have evaluated the introduction of a bifunctional chelator that was attached at ε-NH_2 groups within the molecule. Such conjugated bifunctional chelators may bind to or interfere with regions of the antibody that are mandatory for antigen recognition. Thereby, immunoreactivity and tumor-targeting potential of the radioimmunoconjugate could be adversely affected (*20*). However, the ^{99m}Tc labeling of L19-Hi20 resulted in radiometal chelate conjugates of high immunoreactivity (>80%).

Because the affinity as well as the resulting in vivo targeting properties of antibody fragments may be improved for covalent and associative dimers compared with monomeric derivatives (*21,22*), the formats of our labeling products were evaluated. The scFv L19 has already been described as a mixture of monomer and homodimer (*23*). The ^{99m}Tc-L19 derivatives investigated in this study appeared either as a monomer/dimer mixture (^{99m}Tc-AP39, ^{99m}Tc-L19-Hi20) or as a completely dimeric product (^{99m}Tc-L19-His).

F9 tumors (murine teratocarcinoma) were described to express high levels of ED-B fibronectin (*11,23*) and, therefore, have been used as a tumor model to investigate targeting by L19 and derivatives thereof (*16,24,25*). Biodistribution experiments showed specific tumor uptake of all ^{99m}Tc-L19 derivatives in F9-bearing mice combined with a rapid blood clearance. Elevated uptake in the ovaries and the uterus was regarded as specific targeting of ED-B fibronectin, which is physiologically expressed in reproductive organs (*4,5*). ^{99m}Tc-AP39 demonstrated high tumor uptake, fast excretion, and low background activity comparable with the in vivo data of ^{125}I-L19 in the same tumor model (*10,11*). The resulting tumor-to-tissue ratios (e.g., T/B ratio of 6.3 at 3 h after injection) were even slightly better than those of ^{125}I-L19 (e.g., T/B ratio at 3 h after injection of 1.9 (*10*) and 1.7 (*11*)). The same observation was made by Kang et al. (*26*), who found higher tumor-to-tissue ratios of ^{99m}Tc-scFvs against a high-molecular-weight melanoma–associated antigen compared with ^{125}I-labeled derivatives of these scFvs, with the exception of the kidneys. In comparison,

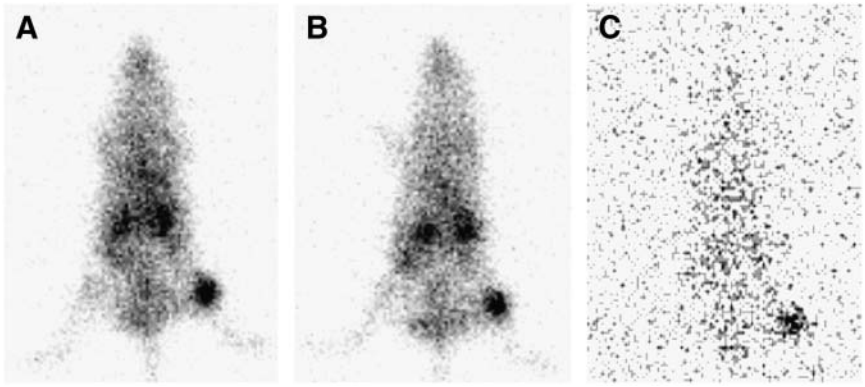

FIGURE 5. Scintigraphic images (posterior) of ^{99m}Tc-AP39 in F9 tumor–bearing mice 3 h (A), 5 h (B), and 24 h (C) after injection.

other ^{99m}Tc-scFvs—for example, against carcinoembryonic antigen—were reported to have much lower T/B ratios of only 4 after 24 h (*27*) or of 2.07 at 4 h after injection into tumor-bearing mice (*28*). Scintigraphic images of F9 tumors by ^{99m}Tc-AP39 can be achieved more rapidly and with a better quality compared with fluorescent images obtained by Cy7-labeled L19 (*25*).

^{99m}Tc-L19-His showed a tumor-targeting potential comparable with that of ^{99m}Tc-AP39 but showed an elevated accumulation of radioactivity in nontarget organs. Its high kidney accumulation is an especially critical issue, resulting in unfavorable background activity in images after 3 and 5 h. High accumulation of radioactivity in the kidneys with His-tagged scFvs when radiolabeled with $[^{99m}Tc(OH_2)_3(CO)_3]^+$ was already described by Waibel et al. (*29*), who found, for an anti–c-erb B2 scFv, a kidney uptake of 108.6 %ID/g after 24 h.

The in vivo targeting properties of ^{99m}Tc-L19-Hi20 were comparable with those of ^{99m}Tc-AP39, as demonstrated by a similar tumor uptake. However, its slower blood kinetics resulted in a high background activity, leading to inferior image quality. This effect was presumably caused by a larger amount of high-molecular-weight impurities as well as the chelator Hi20. It has been suggested that the pharmacokinetic behavior with regard to half-life in the blood and accumulation in nontarget organs may be strongly influenced by chelators conjugated to the protein (*20*).

Besides tumor retention, the most prominent uptake for all three investigated L19 derivatives was observed in the kidney. High kidney uptake is a common observation together with antibody fragments radiolabeled with ^{99m}Tc, ^{111}In, or ^{90}Y. Whereas ^{125}I-labeled proteins are known to be rapidly deiodinated in the kidney (*30*), ^{99m}Tc-scFvs seem to be temporarily trapped by the renal tubular cells after endocytosis (*31*). Besides the isotope itself, kidney uptake of antibody fragments is influenced by the chelator and the linker conjugated to the protein (*32*). However, in contrast to therapy, high uptake in the kidneys is not as problematic because today SPECT enables separation of closely grouped body areas.

CONCLUSION

Three different L19 scFv derivatives designed for labeling with ^{99m}Tc, the SPECT isotope of choice, have been compared. Although these ^{99m}Tc-L19 derivatives still bind equally to ED-B fibronectin in vitro and in vivo, their pharmacokinetic behavior in mice was different. ^{99m}Tc-AP39 showed the most favorable pharmacokinetic and tumor-targeting properties with low concentration of radioactivity

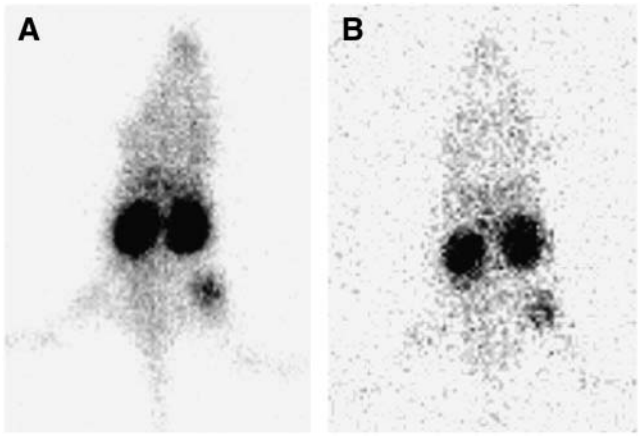

FIGURE 6. Scintigraphic images (posterior) of ^{99m}Tc-L19-His in F9 tumor–bearing mice 5 h (A) and 24 h (B) after injection.

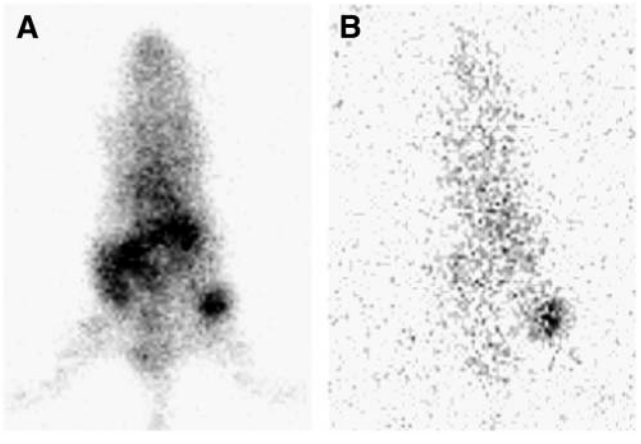

FIGURE 7. Scintigraphic images (posterior) of ^{99m}Tc-L19-Hi20 in F9 tumor–bearing mice 5 h (A) and 24 h (B) after injection.

in the blood, rapid renal excretion, and high in vivo stability for early diagnostic imaging, whereas ^{99m}Tc-L19-His and ^{99m}Tc-L19-Hi20 demonstrated, despite comparable tumor-targeting potential, significant accumulation of radioactivity in the kidneys and other nontarget organs. ^{99m}Tc-AP39 is a most attractive imaging agent for the detection of ED-B fibronectin associated with angiogenesis in actively growing solid tumors and their metastases. Further studies are needed to evaluate the potential of ^{99m}Tc-AP39 both as a stratification marker as well as for early assessment of therapy response.

ACKNOWLEDGMENTS

We thank Eva-Maria Bickel, Marion Szymanski, Sabine Baumann, Ingolf Weber, and Ingo Horn for excellent technical assistance and John Cyr for reviewing the manuscript.

REFERENCES

1. Carmeliet P, Jain RK. Angiogenesis in cancer and other diseases. *Nature.* 2000;407:249–257.
2. Davis DW, McConkey DJ, Abbruzzese JL, Herbst RS. Surrogate markers in antiangiogenesis clinical trials. *Br J Cancer.* 2003;89:8–14.
3. Kosmehl H, Berndt A, Katenkamp D. Molecular variants of fibronectin and laminin: structure, physiological occurrence and histopathological aspects. *Virchows Arch.* 1996;429:311–322.
4. Castellani P, Viale G, Dorcaratto A, et al. The fibronectin isoform containing the ED-B oncofetal domain: a marker of angiogenesis. *Int J Cancer.* 1994;59: 612–618.
5. Carnemolla B, Balza E, Siri A, et al. A tumor-associated fibronectin isoform generated by alternative splicing of messenger RNA precursors. *J Cell Biol.* 1989;108:1139–1148.
6. Kaczmarek J, Castellani P, Nicolo G, Spina B, Allemanni G, Zardi L. Distribution of oncofetal fibronectin isoforms in normal, hyperplastic and neoplastic human breast tissues. *Int J Cancer.* 1994;59:11–16.
7. Pujuguet P, Hammann A, Moutet M, Samuel JL, Martin F, Martin M. Expression of fibronectin ED-A+ and ED-B+ isoforms by human and experimental colorectal cancer: contribution of cancer cells and tumor-associated myofibroblasts. *Am J Pathol.* 1996;148:579–592.
8. Santimaria M, Moscatelli G, Viale GL, et al. Immunoscintigraphic detection of the ED-B domain of fibronectin, a marker of angiogenesis, in patients with cancer. *Clin Cancer Res.* 2003;9:571–579.
9. Pini A, Viti F, Santucci A, et al. Design and use of a phage display library: human antibodies with subnanomolar affinity against a marker of angiogenesis eluted from a two-dimensional gel. *J Biol Chem.* 1998;273:21769–21776.
10. Tarli L, Balza E, Viti F, et al. A high-affinity human antibody that targets tumoral blood vessels. *Blood.* 1999;94:192–198.
11. Borsi L, Balza E, Bestagno M, et al. Selective targeting of tumoral vasculature: comparison of different formats of an antibody (L19) to the ED-B domain of fibronectin. *Int J Cancer.* 2002;102:75–85.
12. Francesconi LC, Zheng Y, Bartis J, Blumenstein M, Costello C, De Rosch MA. Preparation and characterization of [^{99}TcO] apcitide: a technetium labeled peptide. *Inorg Chem.* 2004;43:2867–2875.
13. Alberto R, Schibli R, Egli A, Schubiger AP, Abram U, Kaden TA. A novel organometallic aqua complex of technetium for the labeling of biomolecules: synthesis of $[^{99m}Tc(OH_2)_3(CO)_3]^+$ from $[^{99m}TcO_4]^-$ in aqueous solution and its reaction with a bifunctional ligand. *J Am Chem Soc.* 1998;120(31):7987–7988.
14. Stalteri MA, Bansal S, Hider R, Mather SJ. Comparison of the stability of technetium-labeled peptides to challenge with cysteine. *Bioconjug Chem.* 1999; 10:130–136.
15. Menrad A, Menssen HD. ED-B fibronectin as a target for antibody-based cancer treatments. *Expert Opin Ther Targets.* 2005;9:491–500.
16. Borsi L, Balza E, Carnemolla B, et al. Selective targeted delivery of TNF alpha to tumor blood vessels. *Blood.* 2003;102:4384–4392.
17. Halin C, Gafner V, Villani ME, et al. Synergistic therapeutic effects of a tumor targeting antibody fragment, fused to interleukin 12 and to tumor necrosis factor alpha. *Cancer Res.* 2003;63:3202–3210.
18. Mease RC, Lambert C. Newer methods of labeling diagnostic agents with Tc-99m. *Semin Nucl Med.* 2001;31:278–285.
19. George AJ, Jamar F, Tai MS, et al. Radiometal labeling of recombinant proteins by a genetically engineered minimal chelation site: technetium-99m coordination by single-chain Fv antibody fusion proteins through a C-terminal cysteinyl peptide. *Proc Natl Acad Sci U S A.* 1995;92:8358–8362.
20. Decristoforo C, Mather SJ. The influence of chelator on the pharmacokinetics of ^{99m}Tc-labelled peptides. *Q J Nucl Med.* 2002;46:195–205.
21. Khawli LA, Biela B, Hu P, Epstein AL. Comparison of recombinant derivatives of chimeric TNT-3 antibody for the radioimaging of solid tumors. *Hybrid Hybridomics.* 2003;22:1–9.
22. Pavlinkova G, Beresford GW, Booth BJ, Batra SK, Colcher D. Pharmacokinetics and biodistribution of engineered single-chain antibody constructs of MAb CC49 in colon carcinoma xenografts. *J Nucl Med.* 1999;40:1536–1546.
23. Viti F, Tarli L, Giovannoni L, Zardi L, Neri D. Increased binding affinity and valence of recombinant antibody fragments lead to improved targeting of tumoral angiogenesis. *Cancer Res.* 1999;59:347–352.
24. Hudson PJ, Kortt AA. High avidity scFv multimers; diabodies and triabodies. *J Immunol Methods.* 1999;231:177–189.
25. Neri D, Carnemolla B, Nissim A, et al. Targeting by affinity-matured recombinant antibody fragments of an angiogenesis associated fibronectin isoform. *Nat Biotechnol.* 1997;15:1271–1275.
26. Kang N, Hamilton S, Odili J, Wilson G, Kupsch J. In vivo targeting of malignant melanoma by ^{125}iodine- and ^{99m}technetium-labeled single-chain Fv fragments against high molecular weight melanoma-associated antigen. *Clin Cancer Res.* 2000;6:4921–4931.
27. Verhaar MJ, Keep PA, Hawkins RE, et al. Technetium-99m radiolabeling using a phage-derived single-chain Fv with a C-terminal cysteine. *J Nucl Med.* 1996; 37:868–872.
28. Pietersz GA, Patrick MR, Chester KA. Preclinical characterization and in vivo imaging studies of an engineered recombinant technetium-99m-labeled metallothionein-containing anti-carcinoembryonic antigen single-chain antibody. *J Nucl Med.* 1998;39:47–56.
29. Waibel R, Alberto R, Willuda J, et al. Stable one-step technetium-99m labeling of His-tagged recombinant proteins with a novel Tc(I)-carbonyl complex. *Nat Biotechnol.* 1999;17:897–901.
30. Sharkey RM, Motta-Hennessy C, Pawlyk D, Siegel JA, Goldenberg DM. Biodistribution and radiation dose estimates for yttrium- and iodine-labeled monoclonal antibody IgG and fragments in nude mice bearing human colonic tumor xenografts. *Cancer Res.* 1990;50:2330–2336.
31. Schott ME, Milenic DE, Yokota T, et al. Differential metabolic patterns of iodinated versus radiometal chelated anticarcinoma single-chain Fv molecules. *Cancer Res.* 1992;52:6413–6417.
32. Weber RW, Boutin RH, Nedelman MA, Lister-James J, Dean RT. Enhanced kidney clearance with an ester-linked ^{99m}Tc-radiolabeled antibody Fab′-chelator conjugate. *Bioconjug Chem.* 1990;1:431–437.